The *Drosophila* blood brain barrier is maintained by GPCR-dependent dynamic actin structures

Meital Hatan,[1] Vera Shinder,[2] David Israeli,[1] Frank Schnorrer,[3] and Talila Volk[1]

[1]Department of Molecular Genetics and [2]Department of Chemical Research Support, Weizmann Institute of Science, Rehovot 76100, Israel
[3]Laboratory of Muscle Dynamics, Max Planck Institute of Biochemistry, 82152 Martinsried, Germany

The blood brain barrier (BBB) is essential for insulation of the nervous system from the surrounding environment. In *Drosophila melanogaster*, the BBB is maintained by septate junctions formed between subperineurial glia (SPG) and requires the Moody/G protein–coupled receptor (GPCR) signaling pathway. In this study, we describe novel specialized actin-rich structures (ARSs) that dynamically form along the lateral borders of the SPG cells. ARS formation and association with nonmuscle myosin is regulated by Moody/GPCR signaling and requires myosin activation. Consistently, an overlap between ARS localization, elevated Ca^{2+} levels, and myosin light chain phosphorylation is detected. Disruption of the ARS by inhibition of the actin regulator Arp2/3 complex leads to abrogation of the BBB. Our results suggest a mechanism by which the *Drosophila* BBB is maintained by Moody/GPCR-dependent formation of ARSs, which is supported by myosin activation. The localization of the ARSs close to the septate junctions enables efficient sealing of membrane gaps formed during nerve cord growth.

Introduction

The blood brain barrier (BBB) functions to insulate the central nervous system from its changing molecular environment (Carlson et al., 2000; Abbott et al., 2006). This insulation is essential to defend neurons from toxic substances and to maintain invariable ionic composition within the nervous system to enable efficient neuronal conductivity (Gloor et al., 2001; Zlokovic, 2008). In the vertebrate central nervous system, BBB function depends on an efficient separation between the blood components and the nervous system and is maintained by the sealing of brain endothelial cells by specialized tight junctions (Rubin and Staddon, 1999; Gloor et al., 2001; Zlokovic, 2008). However, insulation of a vertebrate's peripheral nervous system is performed by myelinated Schwann cells that produce a myelin sheath covering the axon in segments separated by the nodes of Ranvier. The segmented myelin sheaths enable saltatory movement of the nerve impulse from node to node (Banerjee and Bhat, 2007; Susuki and Rasband, 2008). The Schwann cell in each myelinated segment forms a continuous array of septate junctions with the underlying axon. These junctions insulate the Na^+ channel–rich domain from the axon segment that undergoes myelination (Spiegel and Peles, 2002).

The *Drosophila melanogaster* BBB is produced by the sealing of the nervous system from the outside surrounding environment by a layer of large glia cells called subperineurial glia (SPG); these cells tightly adhere to each other using an array of septate junctions formed at the lateral borders of these cells (Parker and Auld, 2006; Stork et al., 2008). Similar to vertebrates, sealing of the *Drosophila* nervous system is essential to its protection from toxic substances and high potassium ion concentrations characteristic of the surrounding hemolymph (Mayer et al., 2009). In addition to the membrane proteins NeurexinIV (NrxIV; Baumgartner et al., 1996), Neuroglian (Nrg; Bieber et al., 1989), and Contactin (Falk et al., 2002), *Drosophila* septate junctions contain components of vertebrate tight junctions such as the claudin-like proteins Sinuous (Wu et al., 2004), Megatrachea (Behr et al., 2003), and Kune-kune (Nelson et al., 2010). In the fly, septate junctions functionally replace vertebrate tight junctions to provide an epithelial barrier in various tissues, including the ectoderm, salivary gland, tracheal

Correspondence to Talila Volk: Talila.Volk@weizmann.ac.il

D. Israeli's present address is Mental Health Center, Ashdod 77574, Israel.

Abbreviations used in this paper: ANOVA, analysis of variance; ARS, actin-rich structure; BBB, blood brain barrier; GPCR, G protein–coupled receptor; HPF, high-pressure freezing; MLC, myosin light chain; Nrg, Neuroglian; NrxIV, NeurexinIV; P-MLC, phospho-MLC; SPG, subperineurial glia; Sqh, Spaghetti-squash.

The Rockefeller University Press $30.00
J. Cell Biol. Vol. 192 No. 2 307–319
www.jcb.org/cgi/doi/10.1083/jcb.201007095

cells, and glia cells (Furuse and Tsukita, 2006; Banerjee and Bhat, 2007). The dynamics of septate junction formation have not been elucidated. Specifically, their ability to provide the sealing function during growth and morphogenesis of these distinct tissues is not understood at the structural or the molecular level.

In *Drosophila*, different types of glia cells exhibit differential functions in providing nurture, insulation, and support for the nervous system (Freeman and Doherty, 2006; Parker and Auld, 2006; Stork et al., 2008). The SPG are large cells defined during embryonic development that form a continuous cell layer located between the more external layer of perineurial glia cells and the more internal cortex glia enveloping individual axons or axon bundles within the nerve cord. The SPG layer consists of uniquely large cells that maintain tight adhesion with both the external perineural glia and the more internal cortex glia. Importantly, the SPG cells form tight septate junctions in their lateral intercellular border with neighboring SPG cells to form the BBB (Schwabe et al., 2005; Stork et al., 2008). Although the SPG cells are polarized, they do not exhibit the typical epithelial belt of apical cadherin-mediated adherens junctions and therefore lack the mechanical support that these junctions provide.

To maintain insulation of the brain and nerve cord during development from embryo to adult stages, the septate junctions along the entire circumference of the SPG cells must accommodate the growth and morphological changes of the developing nervous system. SPG cells grow in size to mediate their function in the changing environment without further divisions throughout development. Thus, cross talk between the growing brain and nerve cord and the dynamic formation of septate junctions in the SPG cells would be expected to account for the maintenance of nervous system sealing during development. The precise mechanism regulating septate junction continuity along the changing borders of neighboring SPG cells has yet to be characterized.

The signaling pathway regulated by Moody, a G protein–coupled receptor (GPCR) expressed uniquely by SPG cells, might be related to this function. In *moody* mutant flies, BBB function is disrupted, leading to behavioral abnormalities (Bainton et al., 2005). Ultrastructural analysis revealed that in *moody* mutant embryos, septate junctions are nevertheless established, suggesting that all the elements required for their formation exist within the SPG cells. However, the continuity and length of these junctions along the entire circumference of the SPG cells is disrupted, leading to holes in the seals between neighboring SPG cells and consequently to aberrant BBB function (Schwabe et al., 2005). Based on glial-specific rescue experiments, it was proposed that the Moody/GPCR pathway is involved in the regulation of septate junction continuity along the SPG borders and might act autonomously within these cells. *moody* mutant SPG cells exhibit abnormalities in the actin cytoskeleton (Schwabe et al., 2005). However, the molecular link between Moody signaling, actin skeleton arrangement, and the establishment of elongated septate junctions along the SPG plasma membrane is not clear.

In this study, we describe novel highly dynamic actin-rich structures (ARSs) associated with convoluted membrane extensions detected in close proximity to the septate junctions. Further analysis demonstrated that the formation of the ARSs depends on the Moody signaling pathway as well as on the activity of the actin regulatory Arp2/3 complex and myosin activation. Importantly, ARS disruption leads to discontinuities in the septate junctions along the borders of the SPG cells, abrogating BBB function, similarly to the phenotype observed in *moody* mutants. We suggest that the ARSs support specialized membrane convolutions of the SPG plasma membrane that help to stabilize septate junctions at the lateral borders of the SPG cells.

Results

Specialized ARSs are present along the borders of the SPG cells

To gain insight into the actin cytoskeleton organization of the SPG cells, we expressed moesin-GFP (GMA-GFP) in the SPG cells using a specific Gal4 driver, *moody-gal4*. To analyze the cytoskeletal organization of the SPG cells, we chose to look at nerve cords of third instar larvae (half the way to adult fly development), as at this stage the SPG cells are well defined and do not divide anymore. The moesin-GFP labeling was thus specific for the SPG cells, whereas phalloidin marked the F-actin throughout the entire nerve cord. GFP-positive rounded structures were detected along the lateral borders of the SPG cells. These structures overlapped the phalloidin-labeled regions, suggesting that they contain F-actin (Fig. 1, A–C); we therefore named them ARSs. The diameter of the GFP-positive ARSs was around 1–2 µm, which is significantly larger than typical F-actin distribution in adherens type junctions.

Expression of Lifeact-GFP, a 17-aa actin-binding peptide fused to GFP in the SPG cells, similarly decorated the ARSs. Previous experiments demonstrated that overexpression of Lifeact-GFP does not interfere with actin dynamics (Riedl et al., 2008). Thus, based on the co-distribution of moesin-GFP, Lifeact-GFP, and phalloidin, we concluded that the intercellular border of the SPG cells is characterized by novel ARSs.

To reveal the distribution of the ARSs relative to the plasma membrane of the SPG cells, we expressed a membrane form of GFP (CD8-GFP) within the SPG cells and colabeled the nerve cord with phalloidin (Fig. 1, G–I). High magnification showed that the ARSs were in close proximity to the CD8-GFP–labeled membranes, suggesting that the ARSs accumulate around specialized rounded plasma membrane structures at the intercellular SPG borders. The CD8-GFP labeled additional structures within the SPG cells, including weblike structures located at the basal surfaces of these cells.

We next performed immuno-EM experiments on nerve cords taken from larvae expressing moesin-GFP driven by moody-gal4, using anti-GFP antibodies to label the ARSs (Fig. 2). This approach enabled visualization of the actin distribution specifically in the SPG cells. The nerve cords were fixed and processed by high-pressure freezing (HPF) followed by a freeze substitution procedure, which preserved the antigenicity of the GFP. Ultrathin cross sections of the nerve cord were obtained and labeled with anti-GFP antibody, followed by secondary antibody conjugated to 10-nm gold particles. A low magnification

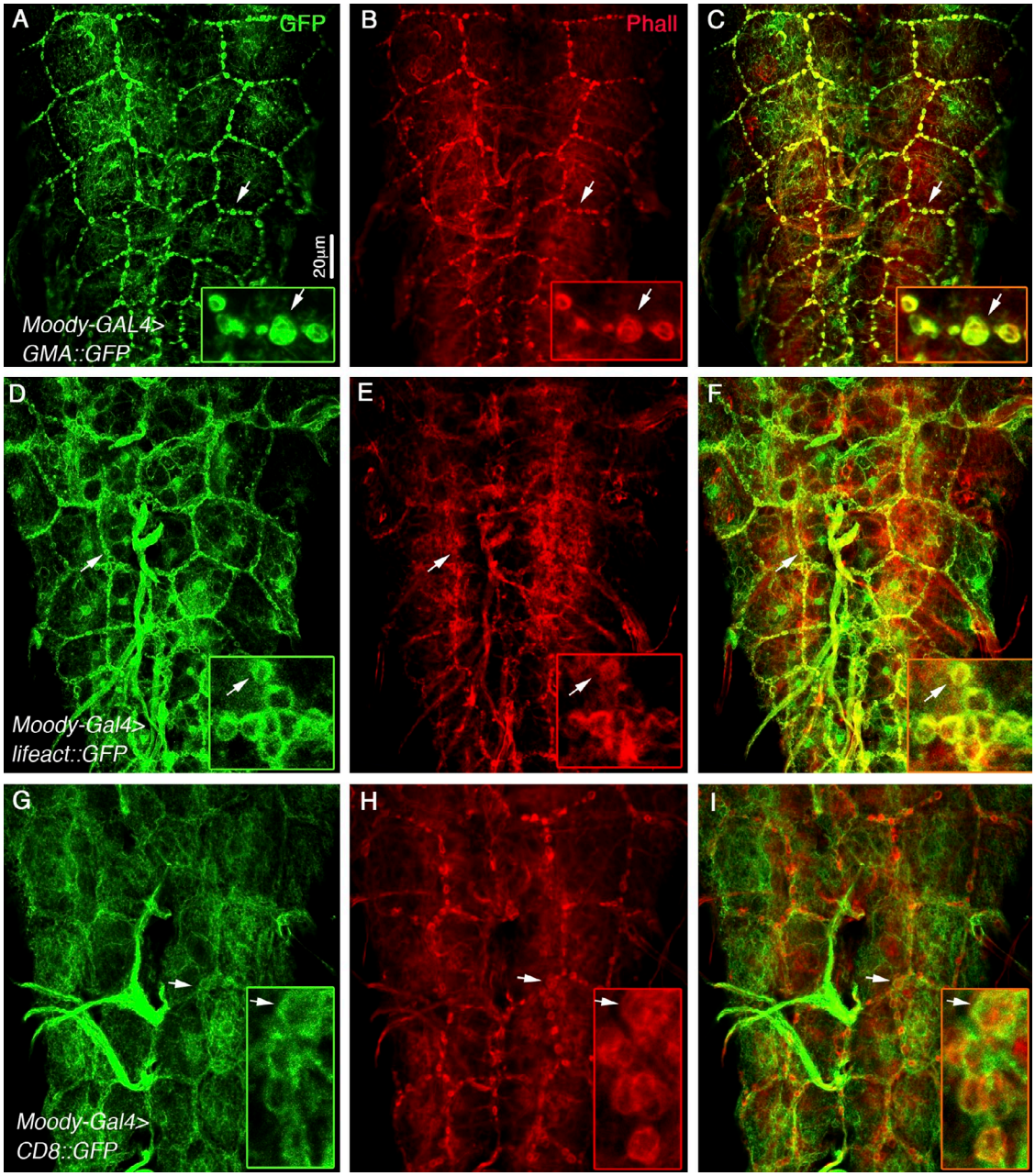

Figure 1. **ARSs are distributed along the SPG intercellular borders.** (A–I) Nerve cords were dissected from third instar larvae, labeled with moesin-GFP (A–C), Lifeact-GFP (D–F), or CD8-GFP (G–I), driven to be expressed in the SPG cells, and then double labeled with phalloidin (Phall). The GFP labeling is shown in A, D, and G, phalloidin in B, E, and H, and their merged images in C, F, and I. The insets in each panel represent high magnification of the region marked by an arrow in the nerve cords. Note that the ARSs are distributed along the borders of the large SPG cells. Overlap between GFP and phalloidin is observed.

of unlabeled cross section through the nerve cord fixed by chemical fixation is shown in Fig. 2 A, indicating the distribution of perineurial (PN), subperineurial (SPG), and axons (N) as well as the elongated septate junctions formed between the SPG cells. A corresponding section in similar orientation and magnification processed by HPF and labeled with anti-GFP is shown in Fig. 2 (B–D). Notice that very close to the site of septate junction (Fig. 2, B and D, arrows) a convoluted rounded membrane extension was labeled with the anti-GFP antibody (see arrows in high magnification in Fig. 2 C). The location, appearance, and size of this structure were similar to that of the ARSs detected by confocal microscopy. Therefore, we suggest that this structure represents an ARS. Notice that the ARS is located next to the septate junction but does not overlap it.

The septate junction components Nrg and Scribble but not NrxIV are associated with the ARSs

Nrg and NrxIV are two membrane proteins essential for proper septate junction formation (Bieber et al., 1989; Baumgartner et al., 1996). To gain insight as to the relationships between the localization of these two proteins and the ARSs, we analyzed

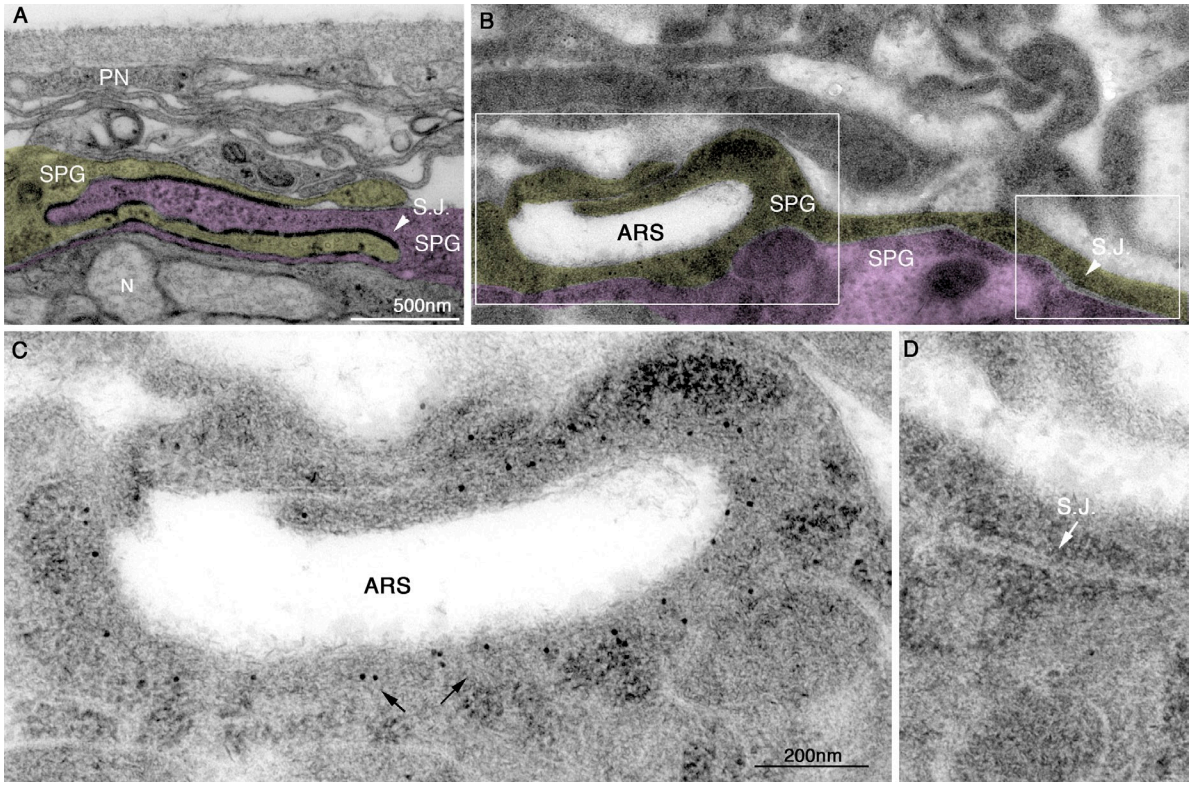

Figure 2. **Ultrastructure of the ARSs labeled with gold-conjugated anti-GFP.** (A–D) Cross sections of nerve cords dissected from third instar larvae carrying moesin-GFP in the SPG cells and processed either by chemical fixation (A) or by HPF followed by freeze substitution (B–D). The perineurial (PN) and subperineurial (SPG) cells (two neighboring SPG cells are marked by yellow or by pink), septate junctions (S.J.), and neurons (N) are indicated in A and B. The nerve cords shown in B–D were labeled with anti-GFP antibody and secondary 10-nm gold–conjugated antibody to visualize moesin-GFP. Low magnification (similar to that in A) of the nerve cord is shown in B, and the two corresponding regions marked in B are shown in higher similar magnification in C and D. The immunogold labeling in C (arrows) is detected very close to the membrane indentation that corresponds to the ARSs. No GFP labeling was detected at the nearby septate junction shown in D (arrow).

their localization relative to phalloidin labeling along the SPG cell borders. To this end, we used two distinct protein trap lines: Nrg-GFP and NrxIV-GFP, in which a GFP fusion protein expressed under the endogenous promoter is formed (Morin et al., 2001; Buszczak et al., 2007). Interestingly, although both proteins are components of the septate junctions, their subcellular distribution along the borders of the SPG cells differed; Nrg was detected in a convoluted distribution at the intercellular SPG borders forming looplike structures, whereas NrxIV was spread along a relatively straight line of the plasma membrane (Fig. 3, A–L). Importantly, these two proteins differed in their degree of association with the ARSs. Nrg often appeared to be surrounded by F-actin, in many cases overlapping the ARSs (Fig. 3, D–F, white arrowheads). In a few cases in which the ARSs were distal to the plasma membrane, no overlap was observed between Nrg and phalloidin (Fig. 3, A–D, open arrowheads). In contrast, NrxIV appeared to be separated from the ARSs, as it did not overlap the phalloidin labeling (Fig. 3, J–L). The fact that Nrg and NrxIV did not always overlap at the SPG membranes suggests that at least one of these proteins does not exhibit restricted localization to septate junctions. Consistent with a previous study suggesting that the distribution of Nrg is not restricted to septate junctions (Hortsch and Margolis, 2003), we observed that the localization of Nrg in the convoluted looplike membranes did not overlap septate junctions. However, the spatial overlapping pattern of Nrg and ARSs suggests their functional association. Interestingly, overexpression of Scribble-GFP, a cytoplasmic component of the septate junctions, also exhibited a distribution that overlapped with the ARSs, similarly to Nrg (Fig. 3, M–O). Collectively, these observations suggest that the membranes along the lateral borders of the SPG form unique convoluted looplike structures, which contain Nrg and Scribble but not NrxIV and are often surrounded by the ARSs.

The ARSs are included within the boundaries of a single SPG cell

The tight lateral association between the cell membranes of neighboring SPG cells did not allow us to determine whether the ARSs are formed on the membranes of two neighboring SPG cells or, alternatively, whether a given ARS originates within a single SPG cell. To address the relationships between the ARSs and the SPG cells, individual glial cells were labeled with GFP by glial-specific Flippase-dependent excision of a genomic spacer localized between a tubulin promoter and GFP (see Materials and methods). Using this method, additional types of individual glia cells were also labeled; however, the SPG cells were easily recognized because of their typical large cubical appearance (Fig. 4 A, arrow). We analyzed the localization of the ARSs, labeled with phalloidin, in individual GFP-labeled SPG cells that were surrounded by non–GFP-labeled SPG.

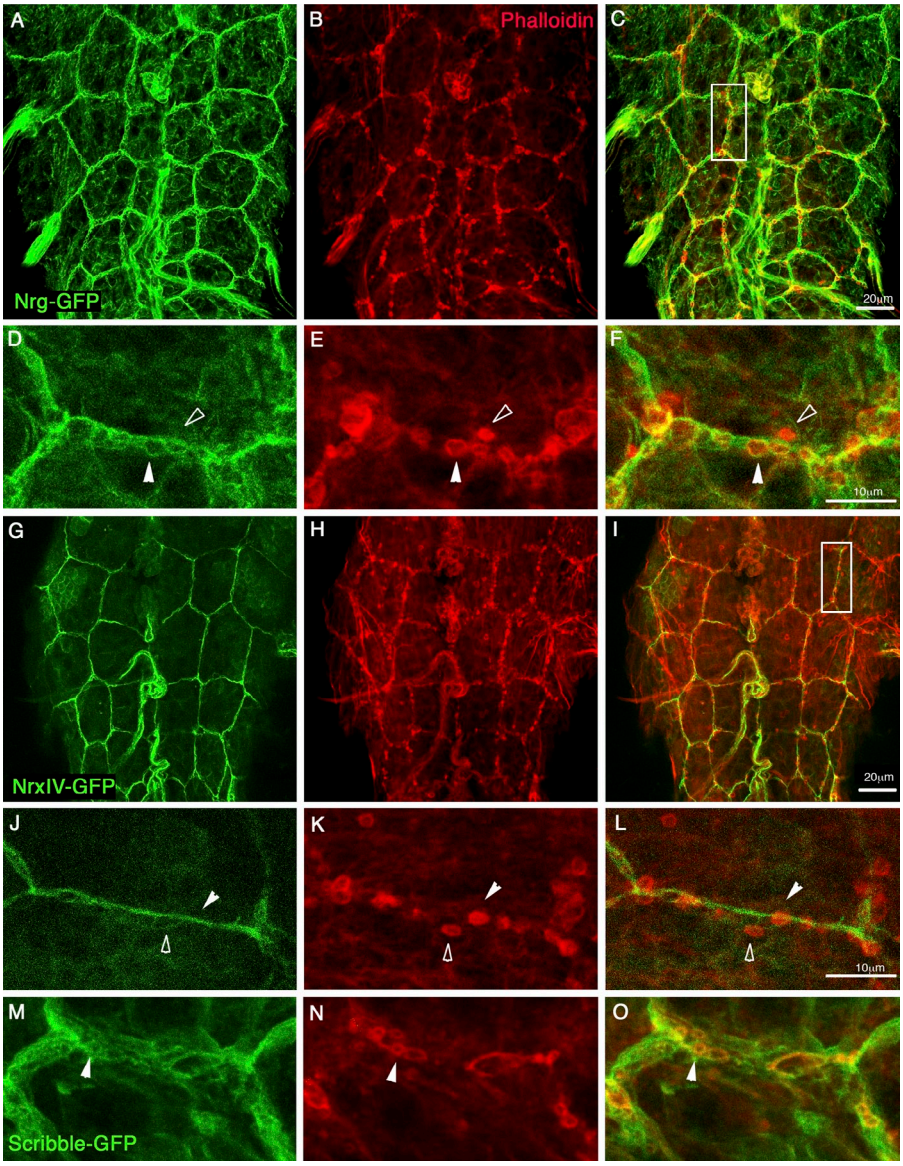

Figure 3. **The ARSs are associated with Nrg-containing membrane loops.** (A–O) Nerve cords dissected from third instar larvae carrying Nrg-GFP (A–F), Nrx-GFP (G–L), or Scribble-GFP (M–O). GFP labeling is shown in A, D, G, J, and M, and the corresponding phalloidin staining is shown in B, E, H, K, and N. The corresponding merged images are shown in C, F, I, L, and O. D–F and J–L show high magnifications of the corresponding area marked with a white rectangle in C and I. Note that the ARSs often overlap the Nrg-GFP labeling (white arrowheads in D–F). In rare cases, we detected an ARS distal from the SPG border that does not overlap Nrg-GFP (open arrowheads in D–F). NrxIV does not overlap the ARSs (white and open arrowheads in J–L). Partial overlap is also noted between Scribble and phalloidin staining (arrowheads in M–O).

In the majority of cases, ARSs were detected within the boundaries of a single GFP-labeled SPG cell (Fig. 4, B–E). We assume that in the few cases in which the relative localization of the ARSs was not clearly visible within a single cell, it was because of the relatively weak GFP expression levels at the edges of the SPG cell, which did not permit adequate identification of the cell borders. Thus, the clonal analysis demonstrated that the ARSs are produced within a single SPG cell, suggesting that at the lateral borders of the SPG cells, the plasma membrane is highly convoluted, forming looplike structures that contain Nrg (but not NrxIV) and are surrounded by F-actin–rich structures as demonstrated in Fig. 4 (F–H).

Cross sections of third instar larvae nerve cords expressing moesin-GFP in the SPG cells and labeled with anti-NrxIV antibody (Fig. 4, F and G) were performed. High magnification of a single confocal optical section shows that the ARSs are located at both sides of the NrxIV-labeled septate junction formed between two neighboring SPG cells, supporting the notion that the ARSs are included within the borders of a single SPG cell and localized in close proximity to the septate junctions as shown in Fig. 2. Moreover, cross sections of nerve cords of larvae carrying Nrg-GFP protein trap and labeled with phalloidin showed that in contrast to NrxIV, Nrg is localized along convoluted membrane indentations that wrap the ARSs (Fig. 4, H and I). To confirm that these membrane indentations are separated from the septate junction site (as was also suggested by the immuno-EM analysis shown in Fig. 2), we labeled nerve cord cross sections from larvae carrying the Nrg-GFP with phalloidin and NrxIV. Whereas NrxIV appeared as a straight line localized between two neighboring SPG cells, corresponding to the septate junction, Nrg-GFP and the ARSs were located proximal to that straight line (Fig. 4, J–L). These results combined with the immuno-EM analysis suggest that the ARSs are located within Nrg-positive membrane convolutions next to the septate junctions at the lateral borders of the SPG cells (Fig. 4 M).

We have excluded the possibility that the ARSs associate with early endosomal compartments, as we did not detect overlapping distribution between the ARSs and Rab-5–GFP in the

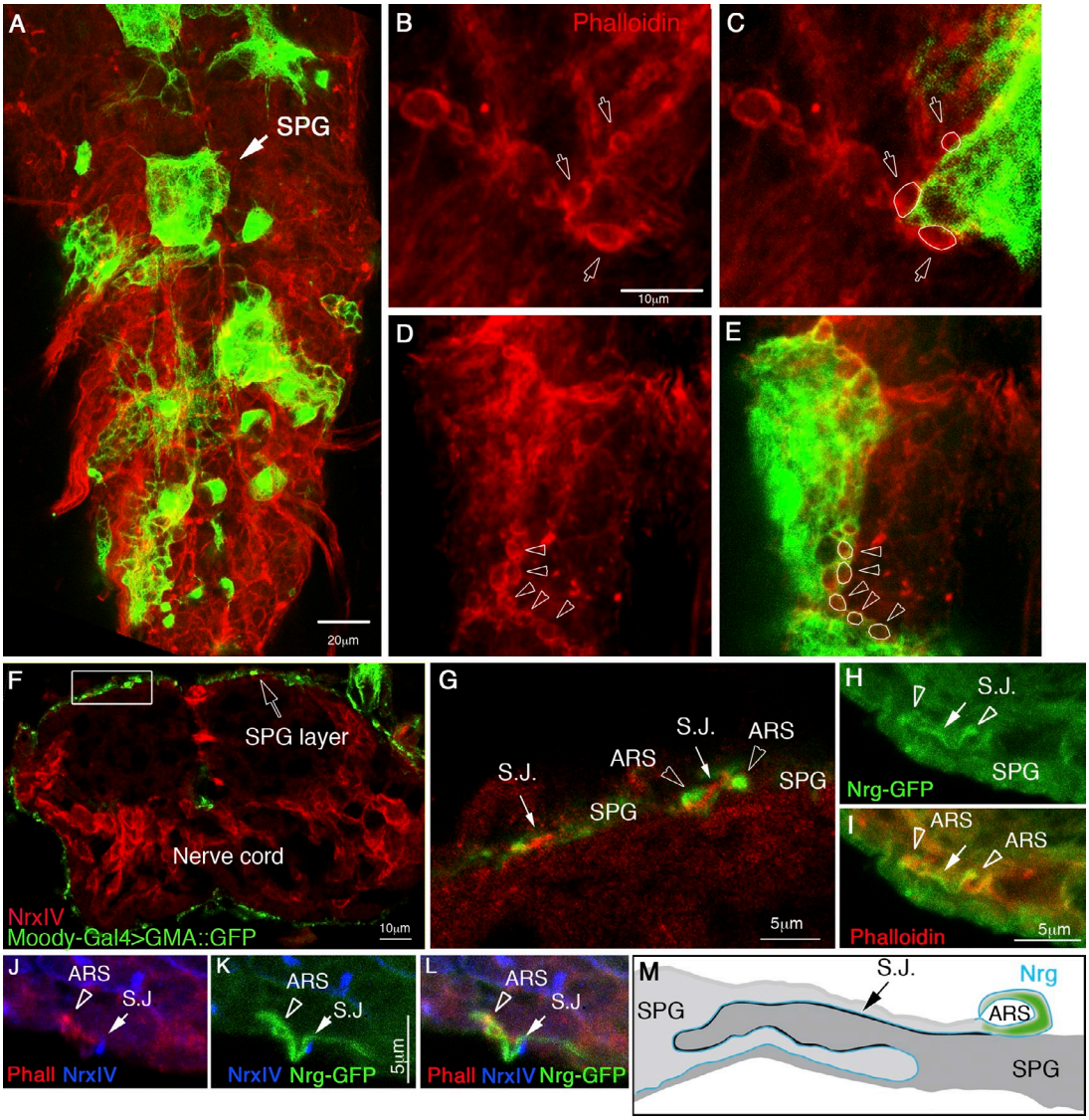

Figure 4. **The relative distribution of the ARSs within a single SPG cell.** Nerve cord dissected from third instar larvae in which single glia cells were labeled with GFP and with phalloidin (e.g., arrow in A). High magnification of the borders between GFP-positive and -negative SPG cells labeled with phalloidin (B and D) or their merged images (C and E) are shown. Arrows in B and C indicate three ARSs that belong to the GFP-negative cell marked by white lines in C. Arrowheads in D and E indicate five ARSs, all of which belong to the GFP-positive SPG cell, marked by white lines in E. (F) A cross section in the nerve cord of third instar larvae carrying moesin-GFP, driven by Moody-Gal4 and stained with anti-NrxIV (red; F and G) and anti-GFP (green; F and G; arrow in F indicates the SPG layer). (G) High magnification of the region marked by the rectangle in F. The septate junction (S.J.) formed between neighboring SPG cells is marked by NrxIV staining (red; arrows). The ARSs are marked by arrowheads. (H and I) High magnification of a cross section of nerve cord dissected from larvae expressing Nrg-GFP (green; H) labeled with phalloidin (red; I). The ARSs are indicated by arrowheads, and the septate junction between neighboring SPG is marked by arrows. J–L show a cross section in Nrg-GFP–expressing larvae labeled with anti-GFP (green; K and L), phalloidin (Phall; red; J and L), and NrxIV (blue; J–L). Arrowheads indicate the ARSs, and arrows show the septate junction. (M) A scheme of the relative distribution of the ARSs, membrane convoluted loop, and septate junction deduced from our analysis.

SPG cells (Fig. S1, D–F). Similarly, the possible association between the ARSs and cellular lipid droplets was excluded as no overlap in the staining of fluorescent nonpolar BODIPY 493/503 (a specific marker for cellular lipid droplets) and phalloidin in the SPG cells was detected (Fig. S1, A–C).

Live imaging of the ARSs reveals their dynamic appearance in wild-type nerve cords

To further characterize the dynamics of the ARSs within the SPG cells, we followed nerve cords of live larvae carrying the moesin-GFP driven by the *moody-gal4*. Third instar larvae were immobilized between two cover slides, and the GFP labeling was analyzed during a 20–30-min period. This analysis revealed that the ARSs are highly dynamic structures; they continuously form and disintegrate (Fig. 5). Interestingly, we detected elevation of ARS number in early pupal stages (1 h after pupal formation; Fig. S2 A). In contrast, in the adult brain, we did not detect typical ARSs (Fig. S2 B), which is consistent with the idea that these structures are more pronounced during brain morphogenesis.

Live larvae simultaneously labeled for F-actin and Nrg using both Lifeact-Ruby driven by *moody-gal4* and Nrg-GFP

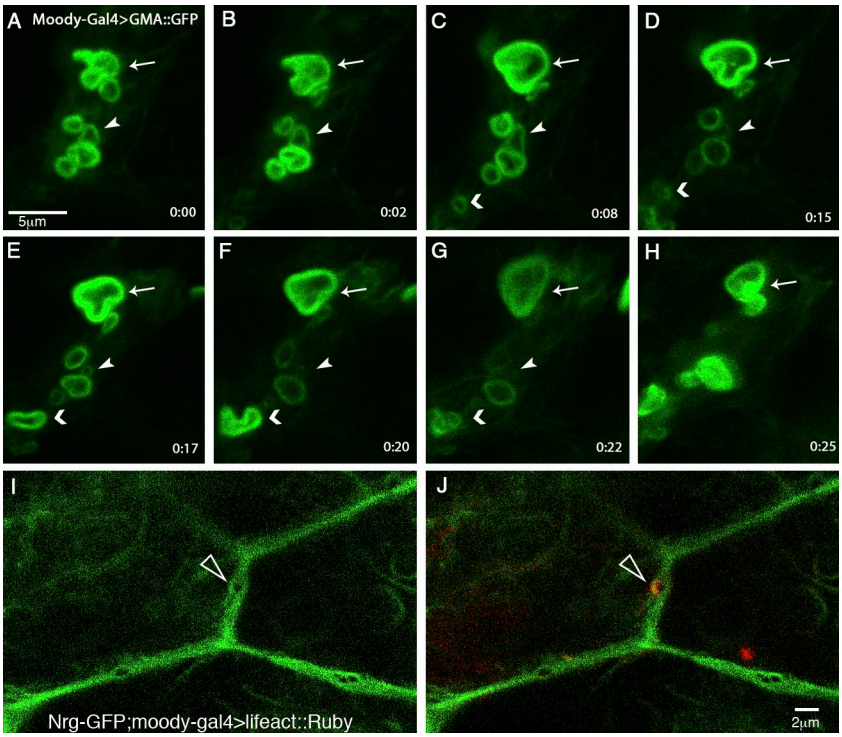

Figure 5. **ARS dynamics in live third instar larvae.** (A–H) GFP images of the ARSs taken at distinct time intervals (in minutes) of the nerve cord of third instar larvae immobilized between two coverslips carrying the moesin-GFP under Moody-Gal4. The arrows and arrowheads indicate to the same ARSs at the different time points. I and J are images of live larvae carrying Nrg-GFP and Lifeact-Ruby driven by Moody-Gal4. An Nrg loop and the ARS associated with it, labeled with Lifeact-Ruby, are indicated (empty arrowheads).

demonstrated partial overlap between the ARSs (red) and the Nrg-GFP convolutions at the intercellular SPG borders (Fig. 5, I and J), similarly to the association shown in fixed nerve cords. These experiments showed that the formation of the ARSs and the Nrg-containing membrane convolutions are highly dynamic and can be detected as well in live preparations.

Disruption of the ARSs leads to abrogated septate junctions and BBB function

To address the molecular basis for ARS formation and its functional significance, the subcellular distribution of the actin regulatory subunit Arp3 was analyzed in SPG cells. Driving Arp3-GFP to SPG cells led to its specific colocalization with the ARSs (Fig. 6, A–C), suggesting that the Arp2/3 complex is specifically recruited to the sites of ARSs and might regulate their formation. Reducing the expression of the Arp2/3 complex using RNAi for both Sop2 and Arp3 subunits of this complex in the SPG cells led to a severe reduction of their size (Fig. 6 D and Fig. S3 G) and number (Fig. 6 D). Temporal restriction of the knockdown of Sop2 and Arp3 to third instar larvae stage (using Gal80^{ts}) led to similar reduction of the ARS size (Fig. S3, A–C). These results suggest that the correct size of the ARSs is regulated by the activity of the Arp2/3 complex, which is localized along the lateral borders of the SPG cells.

ARS size reduction induced by knockdown of Sop2 and Arp3 by RNAi led to gaps in Nrg distribution along the intercellular borders of the SPG cells, and its convoluted structure disappeared (Fig. 6 E). Importantly, the overlap between the Nrg-GFP and the ARSs was eliminated, supporting the hypothesis that the ARSs are essential to maintain septate junctions along the intercellular SPG borders and for Nrg-GFP membrane convolutions. The efficiency of both *Sop2* and *Arp3* RNAi constructs to compromise Arp2/3 function was demonstrated previously (Massarwa et al., 2009). These experiments demonstrate that ARS formation in the SPG cells depends on activation of the Arp2/3 complex, which is recruited to the intercellular SPG borders.

To directly assess the contribution of the ARSs to BBB function, we performed a permeability assay for larvae in which the ARSs were disrupted by SPG-specific knockdown of the Arp2/3 complex. Live larvae were submerged into a solution containing 3-kD fluorescein-dextran for 30 min. The larvae were then dissected and fixed, and dye penetration to the ventral cord was assessed by measuring the fluorescent intensity in the nerve cords using confocal microscopy. The fluorescence intensity was measured in three distinct areas in each nerve cord within a single optical section taken from the ventral cord. As expected, dye penetration was significantly higher in the *moody* mutant compared with wild-type larvae, as demonstrated previously ($n = 12$; $P < 0.0066$; Fig. 6 G; Bainton et al., 2005; Schwabe et al., 2005). Significantly, dye penetration of larvae carrying SPG-dependent RNAi for the Arp2/3 complex was also significantly higher when compared with controls of either larvae carrying RNAi for Arp2/3 alone (arp2/3RNAi/+; Fig. 6 H) or *moody-gal4* alone (*moody-gal4/+*; Fig. 6 H). Comparison of the three groups of nerve cords (Moody-Gal4>Sop2i;Arp3i, Moody-gal4/+, and Sop2i;Arp3i/+) was performed by one-way analysis of variance (ANOVA) with Dunnett's *t* test (using SAS program) to determine the statistical significance of the difference between the experimental group (Moody-Gal4>Sop2i;Arp3i) and the control groups (Moody-gal4/+ or Sop2i;Arp3i/+). The difference between the experimental group and each of the control groups was statistically significant (at $\alpha = 0.05$).

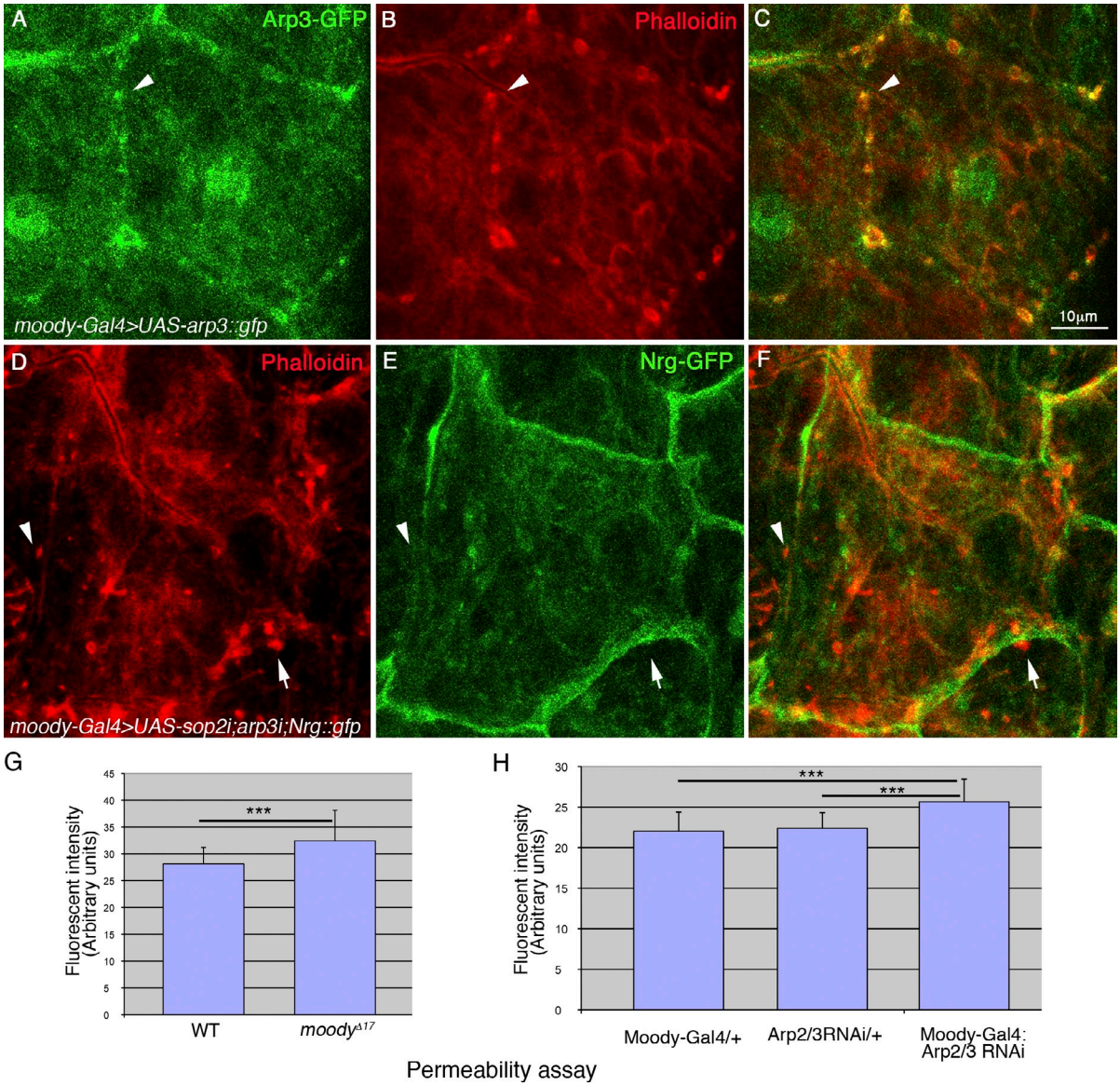

Figure 6. **The Arp2/3 complex is required for ARS formation and for maintenance of BBB function.** (A–C) Nerve cord of third instar larvae expressing Arp3-GFP fusion protein driven by Moody-Gal4. The Arp3-GFP (A) colocalizes with the ARSs labeled with phalloidin (B). The merged image is shown in C. Arrowheads in A–C indicate ARSs colabeled with phalloidin and Arp3-GFP. (D–F) Nerve cord from larvae expressing RNAi for both Arp2 and Arp3 proteins labeled for phalloidin (D). The larvae also carried the Nrg-GFP protein trap. Nrg-GFP is shown in E, and the merged image is shown in F. Arrows show aberrant ARSs that no longer associate with Nrg-GFP labeling. Arrowheads indicate sites lacking Nrg-GFP continuity. (G) Dye penetration to the nerve cord was measured by the fluorescent intensity of nerve cords dissected from wild-type (WT) larvae and compared with *moody* mutant larvae (*moody*$^{\Delta 17}$). The difference between the averaged fluorescent intensity of the two groups was calculated by Student's *t* test and was found to be significant (***, $P < 0.0066$). (H) Dye penetration was compared between three groups: control larvae carrying RNAi to the Arp2/3 components alone (UAS-sop2i;arp3i/+), control larvae carrying *moody-gal4* alone (*moody-gal4/+*), or an experimental group of Arp2/3 knockdown larvae (*moody-gal4:UAS-sop2i;arp3i*). One-way ANOVA test with Dunnett's test (using SAS program) was used to determine the statistical significance of the difference between the experimental and the control groups (Moody-gal4/+ or Sop2i;Arp3i/+). In both cases, the difference between the experimental group and each of the control groups was statistically significant (at $\alpha = 0.05$; indicated by asterisks). (G and H) Error bars indicate standard deviation.

These experiments demonstrate that disruption of the ARSs in the SPG promotes discontinuous appearance of Nrg-GFP along the SPG intercellular borders, leading to the opening of the BBB in a similar fashion as detected in *moody* mutant larvae. Therefore, we suggest that the ARSs provide support for the formation of continuous septate junctions along the entire circumference of the SPG cells, which is essential for the maintenance of the BBB.

Myosin activation is required for ARS formation

The specific F-actin organization of the ARSs might be promoted by myosin contractile activity. To address this possibility, we first characterized the distribution of nonmuscle myosin relative to the ARS in wild-type larval nerve cords. The subcellular distribution of two nonmuscle myosin proteins, Spaghetti-squash (Sqh; nonmuscle myosin regulatory light chain) and

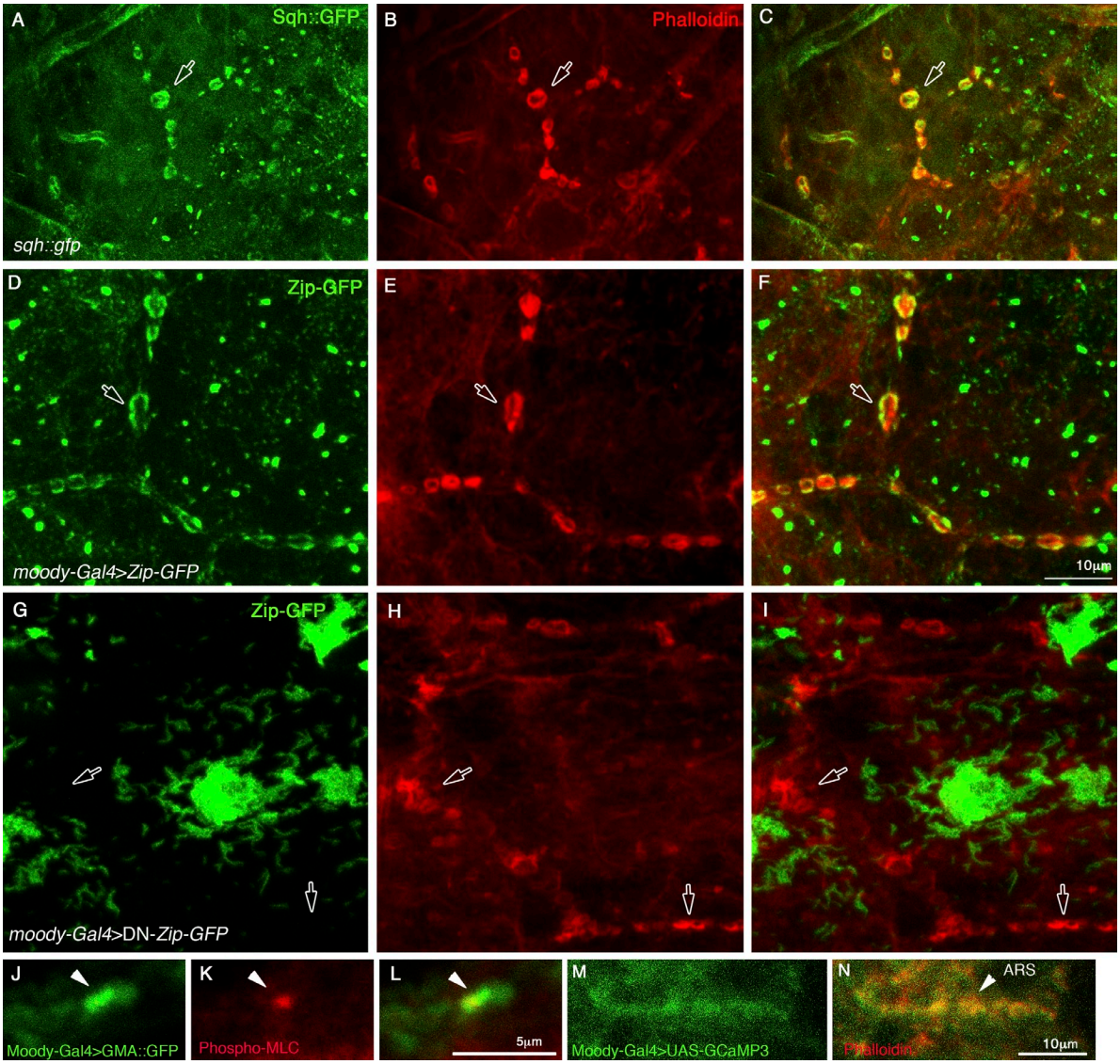

Figure 7. **Activation of nonmuscle myosin is essential for correct morphology of the ARSs.** (A–I) Nerve cords were dissected from third instar larvae carrying MLC Sqh (Sqh-GFP) under its own promoter (A–C) and myosin heavy chain Zipper (Zip-GFP; D–F) or a dominant-negative form of Zipper fused to GFP (DNZip-GFP; G–I) both driven by the Moody-Gal4 driver. A, D, and G show GFP labeling, B, E, and H show phalloidin labeling, and C, F, and I are the corresponding merged images. The arrows in A–F show the ARSs and indicate overlap staining between phalloidin and myosin labeling. The arrows in G show dissociation of Zip-GFP from the ARSs and in H show abnormal morphology of the ARSs. J–L show a cross section of third instar larvae expressing moesin-GFP in SPG cells labeled with anti–P-MLC (red) and GFP. Their merged image is shown in L. An overlap between the ARSs and the P-MLC staining is observed (arrowheads). M and N show the border between two SPG cells of nerve cord dissected from larvae expressing the Ca^{2+} indicator GCaMP3 in SPG cells (M) and labeled with phalloidin (red; N). An overlap between the phalloidin staining representing the ARSs and the fluorescence of the Ca^{2+} indicator is observed (arrowhead).

Zipper (nonmuscle myosin heavy chain), was analyzed using flies carrying Sqh-GFP under its endogenous promoter (Bertet et al., 2004) or UAS-Zipper-GFP (Franke et al., 2005) driven by *moody-gal4* driver. Both myosin-GFP constructs showed specific labeling that was tightly associated with the ARSs at the intercellular SPG borders (Fig. 7, A–F). Interestingly, myosin/GFP labeling appeared to wrap the ARSs.

Importantly, inhibition of Zipper activation by expressing a dominant-negative form of Zipper led to its complete dissociation from the ARSs (Fig. 7 G) and accumulation around the nucleus. Furthermore, dissociation of myosin from the ARSs led to shrinking of the ARSs but did not affect their localization (statistical analysis of the reduction in ARS size is shown in Fig. S3 H). Thus, myosin activation is required to maintain the normal morphology of the ARSs but not their association with the intercellular SPG borders.

Labeled cross sections of nerve cords dissected from larvae expressing moesin-GFP with anti-phospho–myosin light chain (MLC [P-MLC]) showed a specific positive labeling of P-MLC at the ARSs (Fig. 7, J–L). Moreover, in larvae expressing a recently developed sensitized Ca^{2+} indicator, GCaMP3 (Tian et al., 2009), driven to the SPG cells, we detected elevated levels of Ca^{2+} at the ARSs (Fig. 7, M and N). Collectively, these results demonstrate that specific activation of myosin takes place at the ARSs presumably as a result of elevated internal Ca^{2+} levels and that this activation is essential to maintain the ARS size.

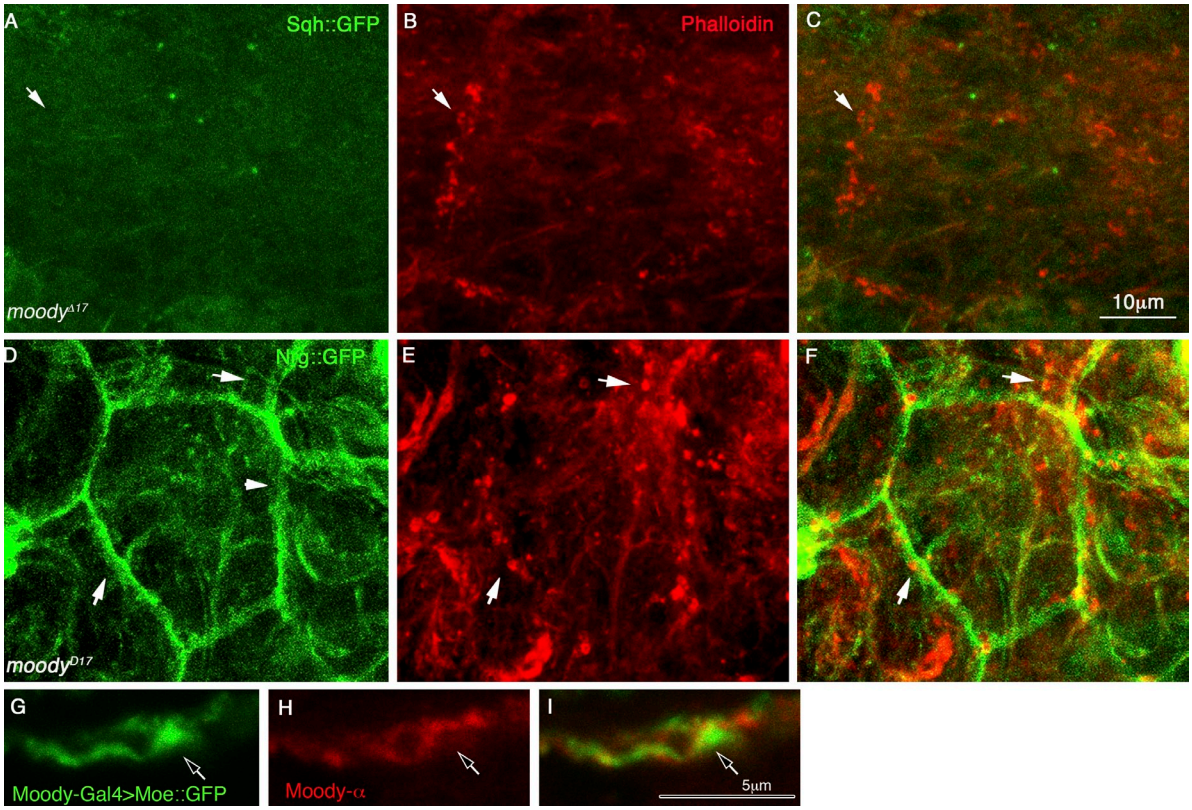

Figure 8. **The Moody/GPCR pathway regulates myosin association with the ARSs.** (A–F) Nerve cords dissected from *moody*$^{\Delta 17}$ mutant larvae and also carrying either Sqh-GFP (A–C) or Nrg-GFP (D–F). GFP labeling is shown in A and D, and phalloidin labeling is shown in B and E. C and F are their corresponding merged images. The arrow in A shows a complete dissociation of Sqh-GFP from the ARS and in B abnormal morphology of the ARSs. The arrowhead in D shows discontinuity of Nrg-GFP labeling, and the arrows in D and E show corresponding locations of abnormal ARS morphology. (G–I) Cross section of third instar larvae nerve cord expressing moesin-GFP and labeled with Moody-α (red). A partial overlap between the moesin-GFP and Moody-α is detected. Moody staining wraps the ARS (arrows).

The Moody/GPCR signaling pathway regulates ARS morphology and association with myosin

To address whether the Moody signaling pathway regulates the morphology of the ARSs, myosin distribution was examined in *moody*$^{\Delta 17}$ mutant nerve cords. In contrast to the association of the Sqh-GFP with the ARSs detected in wild-type larvae nerve cords (Fig. 7 A), it was completely eliminated from the ARSs in *moody*$^{\Delta 17}$ mutant nerve cords (Fig. 8 A). Significantly, in these mutants, the ARSs lost their normal morphology and shrank into small dots that remained localized along the SPG borders (Fig. 8, B and E). This result suggests that the moody pathway regulates the association of nonmuscle myosin with the ARSs. The change in the morphology of the ARSs in *moody* mutant nerve cords might result from their dissociation from the myosin.

As reported previously (Schwabe et al., 2005), the distribution of Nrg-GFP was discontinuous along the lateral intercellular borders of the SPG (Fig. 8 D, arrowhead). In addition, Nrg-GFP distribution lost its convoluted membrane morphology in *moody* mutants, and importantly, there was no overlap between the remaining ARS dots and Nrg-GFP (Fig. 8, D–F, arrows).

These experiments strongly suggest that the Moody/GPCR pathway controls the association of nonmuscle myosin with the ARSs, possibly by inducing phosphorylation of MLC as a result of localized elevation of Ca^{2+} levels. Consistently, Moody-α staining was closely associated with the ARSs but did not entirely overlap these structures (Fig. 8, G–I).

We have attempted to rescue the ARS phenotype in *moody* mutants by expressing UAS–Moody-α or UAS–Moody-β in *moody* mutant larvae. Only partial rescue of the ARSs was detected, presumably because of the sensitivity of the ARSs to Moody levels (Fig. S3, D–F). These results suggest an essential supportive function of the ARSs in the formation of persistent septate junctions along the entire circumference of the SPG cells.

Discussion

The nervous system of the developing fly undergoes significant morphological changes during its development from embryo to adult stages. Surprisingly, the number of the SPG cells does not change (Sepp et al., 2000; Stork et al., 2008). Because these cells maintain the sealing function of the nervous system, we assumed that a mechanism must exist to couple nerve cord growth and the maintenance of septate junctions along the changing borders of the SPG cells. Our analysis suggests that as part of this mechanism, the SPG cells produce specialized convoluted membrane structures that are associated with accumulated F-actin, the ARSs, along their intercellular lateral borders. These structures are highly dynamic and contain Nrg but not NrxIV. Significantly, they are essential for maintaining BBB

function in larval nerve cords, and their maintenance depends on their association with and activation of nonmuscle myosin, which is downstream of Moody/GPCR signaling. Failure to maintain this signaling or direct inhibition of myosin activation leads to dissociation of myosin from the ARSs, shrinking and detachment of the ARSs from the Nrg-positive membrane convolutions, and BBB disruption.

A functional link between the ARSs, *moody/GPCR* signaling, and myosin activation

A previous study (Schwabe et al., 2005) demonstrated that the BBB is disrupted in *moody* mutant embryos. This analysis indicated that although septate junctions are formed in *moody* mutants, their morphology is aberrant. Importantly, in *moody* mutants, the septate junctions were discontinuous along the entire circumference of the SPG cells, leading to abrogation of the BBB. Comparative analysis performed showed that the lack of *moody* leads to a less severe BBB disruption phenotype relative to that of an *NrxIV* mutant, as measured by dye injection assay (Stork et al., 2008). This is presumably because of the fact that in *moody* mutants, septate junctions are formed and part of the BBB function is preserved; however, persistent junction formation at the lateral SPG border is aberrant. These results are consistent with a function for the Moody pathway in the regulation of septate junction continuity.

Our results indicate that *moody* signaling controls the association of the ARSs with membrane convolutions formed along the lateral borders of the SPG cells. Disruption of the ARSs by expression of RNAi against the Arp2/3 components abrogated BBB function to a similar extent as that of *moody* mutants. We suggest a model in which Moody/GPCR signaling promotes myosin activation and association with the ARSs. GPCR signaling often leads to activation of myosin contraction in different cellular/developmental contexts because of a transient release of internal Ca^{2+} pools (Blaser et al., 2006; Turu and Hunyady, 2010). Indeed, we detected elevation of Ca^{2+} levels at the ARS sites. Activation of myosin is essential to preserve ARS morphology and may promote their dynamic behavior. How this behavior relates to the persistent appearance of septate junctions along the lateral SPG borders is yet to be determined. The correlation between the disruption of the ARSs and elimination of the Nrg-positive membrane convolutions is consistent with the idea that the ARSs provide mechanical support for these structures. We hypothesize that these Nrg-positive membrane convolutions are essential for the fast reconstitution of septate junctions during nerve cord growth and morphogenesis. Consistently, lack of the ARSs leads to discontinuity in the appearance of septate junctions as well as abrogation of BBB function. Because some of the ARSs were still detected at the SPG cellular borders in *moody* mutant larvae, we suggest that a Moody-independent mechanism promotes ARS formation at the SPG cellular borders. The Moody/GPCR pathway then maintains their morphology and association with septate junction components by regulation of myosin activation.

The ARSs are unique structures of the SPG cell

The ARSs are novel structures and have not been previously described. One possible explanation is that these are highly delicate structures and might disintegrate during fixation. We suspect that the association of the moesin-GFP with the ARSs led to their stabilization, enabling their visualization both in fixed and live nerve cords. Indeed, when staining wild-type larvae nerve cords only with phalloidin, fewer ARSs were detected; however, their presence was clearly observed in third instar larvae. Moreover, we also detected ARSs using Lifeact-GFP. Two additional types of F-actin structures were detected in SPG cells, apical stress fibers arranged in an anterior posterior polarity and basal weblike stress fibers forming large circles of F-actin. The function of this basal F-actin network as well as its possible contribution to BBB maintenance is yet to be elucidated.

An interesting feature of the ARSs is their association with the plasma membrane. Because the SPG cells do not exhibit a typical epithelial-like belt of apical adherens junctions, we suspect that the ARSs instead provide mechanical support for the intercellular septate junctions formed along the SPG intercellular borders. In summary, we have described novel ARSs involved in the maintenance of convoluted Nrg-positive membrane indentations in the SPG cells, which are essential for maintaining septate junctions between neighboring SPG cells.

In vertebrates' peripheral nervous system, myelinated Schwann cells form a myelin sheath that wraps the axon in segments separated by the nodes of Ranvier. The segmented myelin sheaths enable saltatory movement of the nerve impulse from node to node. The myelin membrane of the Schwann cell forms convoluted loops at the paranodal region separating between the Na^+ channels at the node of Ranvier and the juxtaparanodal K^+ channels located along the paranodal loops (Spiegel and Peles, 2002). These paranodal loops form septate junctions with the axonal membrane, enabling separation between the electrical activity at the node of Ranvier and the internodal region. Whereas the precise cytoskeletal composition of the paranodal loops as well as potential signaling involved in their formation is yet to be elucidated, the convoluted looplike structures of the ARSs in *Drosophila* SPG cells are structurally reminiscent of these paranodal loops, which are associated with the septate junctions. It remains to be elucidated whether similar GPCR-dependent molecular signaling mediates the formation of vertebrate peripheral nervous system paranodal loops and axoglial septate junctions.

Materials and methods

Fly strains

The following fly strains were obtained from published sources: UAS-GCaMP3 (Tian et al., 2009), UAS–Moody-α–GFP and UAS–Moody-β–GFP (Mayer et al., 2009), UAS-GMA-GFP (Kiehart et al., 2000), UAS-Zipper-GFP and UAS-Zipper^{DN}-GFP (Franke et al., 2005), *moody-gal4* and Repo-flp1/Cyo; tub >6k> gal4-UAS-GFP/TM6 (C. Klämbt, University of Münster, Münster, Germany) and *moody*$^{\Delta 17}$ (Bainton et al., 2005), UAS-Lifeact-GFP (F. Schnorrer), UAS-CD8-GFP (Lee and Luo, 1999), Nrg-GFP (Morin et al., 2001), Neurexin-GFP (Edenfeld et al., 2006), UAS-Scribble-GFP (Zeitler et al., 2004), Wasp^{DN} (Tal et al., 2002), arp3-GFP (Hudson and Cooley, 2002), and UAS-sop2RNAi;UAS-arp3RNAi (E. Schejter, Weizmann Institute of Science, Rehovot, Israel). RNAi knockdown strains

Sp2 (VDRC42172) and Arp3 (VDRC35260) were obtained from the Vienna Drosophila RNAi Center stock center (Vienna, Austria).

Tub-gal80^{ts}/+;Moody-Myr-RFP/UAS-sop2RNAi,UAS-arp3RNAi was obtained by crossing the lines Tub-gal80^{ts}/Tub-gal80^{ts};TM2/TM6 (Bloomington Stock Center, Bloomington, IN) and UAS-Zip-GFP/Cyo; Moody-Myr-RFP/TM6 to create Tub-gal80/UAS-Zip-GFP; Moody-Myr-RFP/TM6. These flies were crossed with UAS-sop2RNAi, UAS-arp3RNAi/TM6. All crosses were kept at 25°C. Embryos of the latter cross were moved to 18°C until they reached second instar larvae stage. Third instar larvae were moved to 29°C for 24 h and then dissected and stained for FITC-phalloidin. For the rescue experiment, females of the genotype *moody*$^{\Delta 17}$*/FM7(Blue balancer);Moody-Gal4/Cyo* were crossed to males homozygous for UAS–Moody-α–GFP or UAS–Moody-β–GFP, and the GFP-positive *moody* mutant larvae males were labeled with phalloidin and examined.

Immunohistochemistry and imaging

Larvae nerve cords and brains were dissected in PBSX1.66 and fixed in 6.4% PFA for 20 min. The nerve cords were then washed twice for 10 min in PBS containing 0.1% Triton X-100 (PBT) and were immersed in 80% glycerol solution for 10 min. Then the nerve cords and brains were further cleaned to remove fat and other tissues and mounted on a slide with Aqua-mount (Thermo Fisher Scientific).

For staining with TRICT-phalloidin (P1951; Sigma-Aldrich) or FITC-phalloidin (P5282; Sigma-Aldrich), fixed nerve cords were incubated with phalloidin (1:200) diluted in PBT (from a stock of 1 mg/ml phalloidin solubilized in methanol) for 1 h and then washed four times for 10 min with PBT. Lipid droplet staining was performed using BODIPY 493/503 (D3922; Invitrogen). Larvae nerve cords were dissected in PBSX1.66 and fixed in 6.4% PFA for 20 min. After two washes of 10 min in PBT, the larvae were put in 30% glycerol with BODIPY diluted to 5 µg/ml for 15 min. The brains were dissected and mounted using glycerol 30%. Live imaging was performed as follows: live third instar larvae were placed between two coverslips, which were glued together with gel glue and imaged for 0.5–2 h.

For staining of nerve cord cross sections, larvae nerve cords were dissected and fixed as described in the beginning of this section and then incubated in 10% sucrose solution until they sunk. Nerve cords were moved to 30% sucrose solution for 1 h, arranged in a mold, and frozen in OCT. Cross sections of 8 µm were obtained using a cryostat (CM3050S; Leica). After several washes with PBS, samples were incubated with permeabilization solution (0.25% Triton X-100 and 1% BSA in PBS) for 15 min and blocked with 10% BSA for 1 h. Samples were transferred into primary antibody and incubated overnight at 4°C. After additional washes in PBS, samples were incubated with secondary antibody for 1 h, washed with PBS, and mounted in Aqua-mount. The following primary antibodies were used: rabbit anti-NrxIV (1:1000; C. Klämbt), rabbit anti–Moody-α (1:70; R.J. Bainton, School of Medicine, University of California, San Francisco, San Francisco, CA), rabbit anti–P-MLC2 (1:70; Cell Signaling Technology), and chick anti-GFP (1:70; Aves Laboratories). Secondary antibodies used were as follows: Cy5 anti–rabbit, Cy2 anti–chick, and Cy3 anti–rabbit (Jackson ImmunoResearch Laboratories, Inc.). Both intact nerve cords and sections were mounted with Aqua-mount. All confocal images were acquired at room temperature using an LSM 710 system (Carl Zeiss, Inc.). Intact nerve cord images were taken using 40×/1.20 water immersion lens, and nerve cord cross sections were taken using 63×/1.40 oil immersion lens.

HPF and immunogold labeling for EM

Larvae carrying GMA-GFP under the control of moody-gal4 were dissected in cacodylate buffer and fixed in 0.1% glutaraldehyde. HPF was performed in a Bal-Tec HPM10 apparatus. Frozen samples were transferred to the AFS (Leica) and freeze substituted in acetone, containing 0.1% glutaraldehyde and 0.1% uranylacetate at −90°C for 72 h. The samples were washed in series of the alcohols and embedded in HM20 resin at −30°C. Ultrathin sections (70–90-nm thickness) were prepared with Ultramicrotome UCT (Leica) collected on Ni grids coated with formvar, analyzed under 120 kV on a transmission electron microscope (Tecnai Biotwin Spirit; FEI) and digitized with a charge-coupled device camera (EAGLE; FEI) using TIA software (FEI). For immunogold labeling, the ultrathin sections were washed with PBS + 0.2% glycine. After 20 min of blocking using 0.1% glycine, 0.1% Tween 20, and 1% BSA in PBS, anti-GFP was added in the blocking buffer and incubated for 1.5–2 h at room temperature or overnight. The anti–rabbit conjugated to 10-nm gold particles was added at 1:20 dilution in the blocking buffer for 30 min at room temperature and then washed once by PBS and another six times in H_2O.

Dye penetration assay

Third instar larvae were placed in fluorescein-dextran (3 kD, 10 mg/ml; Invitrogen) diluted 1:50 for 30 min. The larvae were dissected immediately and fixed as described in Immunohistochemistry and imaging, and the nerve cords and brains were dissected and analyzed by an LSM 710 system for fluorescent intensity. Dye penetration was quantified using ImageJ (National Institutes of Health). A single optical section from each nerve cord was examined, three equal-sized areas were selected and averaged for their mean pixel intensity, and background intensity was subtracted. The light intensity of the areas taken from each larva was averaged. For each experiment, 3–10 larvae were analyzed. The statistics were calculated in the following manner: for comparing permeability of *moody*$^{\Delta 17}$ with wild-type, we have used Student's *t* test, and the p-value in this assay was $P < 0.0066$. For comparing the three groups of nerve cords (Moody-Gal4>Sop2i;Arp3i, Moody-gal4/+, and Sop2i;Arp3i/+), we used a one-way ANOVA test with Dunnett's test (using SAS program) to determine the statistical significance of the difference between the experimental group (Moody-Gal4>Sop2i;Arp3i) and the control groups (Moody-gal4/+ or Sop2i;Arp3i/+). In both cases, the difference between the experimental group and each of the control groups was statistically significant (at $\alpha = 0.05$).

Online supplemental material

Fig. S1 shows that there is no overlap between the distribution of the ARSs and lipid droplets (labeled with BODIPY) or with Rab-5–associated endosomes. Fig. S2 shows enrichment of the ARSs in pupal but not in adult fly brains. Fig. S3 shows that temporal knockdown of Arp2/3 only during the third instar larvae stage leads to aberrant ARSs and includes statistical analysis of ARS size after Apr2/3 knockdown after expression of dominant-negative Zipper. Online supplemental material is available at http://www.jcb.org/cgi/content/full/jcb.201007095/DC1.

We thank C. Klämbt, R.J. Bainton, L. Cooley, D. Bilder, R. Wedlich-Soldner, L. Looger, D. Kiehart, and the Bloomington Stock Center for various fly lines and reagents. The EM experiments were conducted at the Irving and Cherna Moskowitz Center for Nano and Bio-Nano Imaging at the Weizmann Institute of Science. In addition, we thank C. Klämbt, R.J. Bainton, E. Schejter, and L. Gilboa for fruitful discussions and critical reading of the manuscript and S. Schwarzbaum for English editing.

This study was supported by a grant from the Minerva Foundation with funding from the Federal German Ministry for Education and Research to T. Volk.

Submitted: 19 July 2010
Accepted: 16 December 2010

References

Abbott, N.J., L. Rönnbäck, and E. Hansson. 2006. Astrocyte-endothelial interactions at the blood-brain barrier. *Nat. Rev. Neurosci.* 7:41–53. doi:10.1038/nrn1824

Bainton, R.J., L.T. Tsai, T. Schwabe, M. DeSalvo, U. Gaul, and U. Heberlein. 2005. moody encodes two GPCRs that regulate cocaine behaviors and blood-brain barrier permeability in *Drosophila*. *Cell*. 123:145–156. doi:10.1016/j.cell.2005.07.029

Banerjee, S., and M.A. Bhat. 2007. Neuron-glial interactions in blood-brain barrier formation. *Annu. Rev. Neurosci.* 30:235–258. doi:10.1146/annurev.neuro.30.051606.094345

Baumgartner, S., J.T. Littleton, K. Broadie, M.A. Bhat, R. Harbecke, J.A. Lengyel, R. Chiquet-Ehrismann, A. Prokop, and H.J. Bellen. 1996. A *Drosophila* neurexin is required for septate junction and blood-nerve barrier formation and function. *Cell*. 87:1059–1068. doi:10.1016/S0092-8674(00)81800-0

Behr, M., D. Riedel, and R. Schuh. 2003. The claudin-like megatrachea is essential in septate junctions for the epithelial barrier function in *Drosophila*. *Dev. Cell*. 5:611–620. doi:10.1016/S1534-5807(03)00275-2

Bertet, C., L. Sulak, and T. Lecuit. 2004. Myosin-dependent junction remodelling controls planar cell intercalation and axis elongation. *Nature*. 429:667–671. doi:10.1038/nature02590

Bieber, A.J., P.M. Snow, M. Hortsch, N.H. Patel, J.R. Jacobs, Z.R. Traquina, J. Schilling, and C.S. Goodman. 1989. *Drosophila* neuroglian: a member of the immunoglobulin superfamily with extensive homology to the vertebrate neural adhesion molecule L1. *Cell*. 59:447–460. doi:10.1016/0092-8674(89)90029-9

Blaser, H., M. Reichman-Fried, I. Castanon, K. Dumstrei, F.L. Marlow, K. Kawakami, L. Solnica-Krezel, C.P. Heisenberg, and E. Raz. 2006.

Migration of zebrafish primordial germ cells: a role for myosin contraction and cytoplasmic flow. *Dev. Cell*. 11:613–627. doi:10.1016/j.devcel.2006.09.023

Buszczak, M., S. Paterno, D. Lighthouse, J. Bachman, J. Planck, S. Owen, A.D. Skora, T.G. Nystul, B. Ohlstein, A. Allen, et al. 2007. The carnegie protein trap library: a versatile tool for *Drosophila* developmental studies. *Genetics*. 175:1505–1531. doi:10.1534/genetics.106.065961

Carlson, S.D., J.L. Juang, S.L. Hilgers, and M.B. Garment. 2000. Blood barriers of the insect. *Annu. Rev. Entomol.* 45:151–174. doi:10.1146/annurev.ento.45.1.151

Edenfeld, G., G. Volohonsky, K. Krukkert, E. Naffin, U. Lammel, A. Grimm, D. Engelen, A. Reuveny, T. Volk, and C. Klämbt. 2006. The splicing factor crooked neck associates with the RNA-binding protein HOW to control glial cell maturation in *Drosophila*. *Neuron*. 52:969–980. doi:10.1016/j.neuron.2006.10.029

Falk, J., C. Bonnon, J.A. Girault, and C. Faivre-Sarrailh. 2002. F3/contactin, a neuronal cell adhesion molecule implicated in axogenesis and myelination. *Biol. Cell*. 94:327–334. doi:10.1016/S0248-4900(02)00006-0

Franke, J.D., R.A. Montague, and D.P. Kiehart. 2005. Nonmuscle myosin II generates forces that transmit tension and drive contraction in multiple tissues during dorsal closure. *Curr. Biol.* 15:2208–2221. doi:10.1016/j.cub.2005.11.064

Freeman, M.R., and J. Doherty. 2006. Glial cell biology in *Drosophila* and vertebrates. *Trends Neurosci.* 29:82–90. doi:10.1016/j.tins.2005.12.002

Furuse, M., and S. Tsukita. 2006. Claudins in occluding junctions of humans and flies. *Trends Cell Biol.* 16:181–188. doi:10.1016/j.tcb.2006.02.006

Gloor, S.M., M. Wachtel, M.F. Bolliger, H. Ishihara, R. Landmann, and K. Frei. 2001. Molecular and cellular permeability control at the blood-brain barrier. *Brain Res. Brain Res. Rev.* 36:258–264. doi:10.1016/S0165-0173(01)00102-3

Hortsch, M., and B. Margolis. 2003. Septate and paranodal junctions: kissing cousins. *Trends Cell Biol.* 13:557–561. doi:10.1016/j.tcb.2003.09.004

Hudson, A.M., and L. Cooley. 2002. A subset of dynamic actin rearrangements in *Drosophila* requires the Arp2/3 complex. *J. Cell Biol.* 156:677–687. doi:10.1083/jcb.200109065

Kiehart, D.P., C.G. Galbraith, K.A. Edwards, W.L. Rickoll, and R.A. Montague. 2000. Multiple forces contribute to cell sheet morphogenesis for dorsal closure in *Drosophila*. *J. Cell Biol.* 149:471–490. doi:10.1083/jcb.149.2.471

Lee, T., and L. Luo. 1999. Mosaic analysis with a repressible cell marker for studies of gene function in neuronal morphogenesis. *Neuron*. 22:451–461. doi:10.1016/S0896-6273(00)80701-1

Massarwa, R., E.D. Schejter, and B.Z. Shilo. 2009. Apical secretion in epithelial tubes of the *Drosophila* embryo is directed by the Formin-family protein Diaphanous. *Dev. Cell*. 16:877–888. doi:10.1016/j.devcel.2009.04.010

Mayer, F., N. Mayer, L. Chinn, R.L. Pinsonneault, D. Kroetz, and R.J. Bainton. 2009. Evolutionary conservation of vertebrate blood-brain barrier chemoprotective mechanisms in *Drosophila*. *J. Neurosci.* 29:3538–3550. doi:10.1523/JNEUROSCI.5564-08.2009

Morin, X., R. Daneman, M. Zavortink, and W. Chia. 2001. A protein trap strategy to detect GFP-tagged proteins expressed from their endogenous loci in *Drosophila*. *Proc. Natl. Acad. Sci. USA*. 98:15050–15055. doi:10.1073/pnas.261408198

Nelson, K.S., M. Furuse, and G.J. Beitel. 2010. The *Drosophila* Claudin Kunekune is required for septate junction organization and tracheal tube size control. *Genetics*. 185:831–839. doi:10.1534/genetics.110.114959

Parker, R.J., and V.J. Auld. 2006. Roles of glia in the *Drosophila* nervous system. *Semin. Cell Dev. Biol.* 17:66–77. doi:10.1016/j.semcdb.2005.11.012

Riedl, J., A.H. Crevenna, K. Kessenbrock, J.H. Yu, D. Neukirchen, M. Bista, F. Bradke, D. Jenne, T.A. Holak, Z. Werb, et al. 2008. Lifeact: a versatile marker to visualize F-actin. *Nat. Methods*. 5:605–607. doi:10.1038/nmeth.1220

Rubin, L.L., and J.M. Staddon. 1999. The cell biology of the blood-brain barrier. *Annu. Rev. Neurosci.* 22:11–28. doi:10.1146/annurev.neuro.22.1.11

Schwabe, T., R.J. Bainton, R.D. Fetter, U. Heberlein, and U. Gaul. 2005. GPCR signaling is required for blood-brain barrier formation in *Drosophila*. *Cell*. 123:133–144. doi:10.1016/j.cell.2005.08.037

Sepp, K.J., J. Schulte, and V.J. Auld. 2000. Developmental dynamics of peripheral glia in *Drosophila melanogaster*. *Glia*. 30:122–133. doi:10.1002/(SICI)1098-1136(200004)30:2<122::AID-GLIA2>3.0.CO;2-B

Spiegel, I., and E. Peles. 2002. Cellular junctions of myelinated nerves (Review). *Mol. Membr. Biol.* 19:95–101. doi:10.1080/09687680210130009

Stork, T., D. Engelen, A. Krudewig, M. Silies, R.J. Bainton, and C. Klämbt. 2008. Organization and function of the blood-brain barrier in *Drosophila*. *J. Neurosci.* 28:587–597. doi:10.1523/JNEUROSCI.4367-07.2008

Susuki, K., and M.N. Rasband. 2008. Molecular mechanisms of node of Ranvier formation. *Curr. Opin. Cell Biol.* 20:616–623. doi:10.1016/j.ceb.2008.09.007

Tal, T., D. Vaizel-Ohayon, and E.D. Schejter. 2002. Conserved interactions with cytoskeletal but not signaling elements are an essential aspect of *Drosophila* WASp function. *Dev. Biol.* 243:260–271. doi:10.1006/dbio.2002.0571

Tian, L., S.A. Hires, T. Mao, D. Huber, M.E. Chiappe, S.H. Chalasani, L. Petreanu, J. Akerboom, S.A. McKinney, E.R. Schreiter, et al. 2009. Imaging neural activity in worms, flies and mice with improved GCaMP calcium indicators. *Nat. Methods*. 6:875–881. doi:10.1038/nmeth.1398

Turu, G., and L. Hunyady. 2010. Signal transduction of the CB1 cannabinoid receptor. *J. Mol. Endocrinol.* 44:75–85. doi:10.1677/JME-08-0190

Wu, V.M., J. Schulte, A. Hirschi, U. Tepass, and G.J. Beitel. 2004. Sinuous is a *Drosophila* claudin required for septate junction organization and epithelial tube size control. *J. Cell Biol.* 164:313–323. doi:10.1083/jcb.200309134

Zeitler, J., C.P. Hsu, H. Dionne, and D. Bilder. 2004. Domains controlling cell polarity and proliferation in the *Drosophila* tumor suppressor Scribble. *J. Cell Biol.* 167:1137–1146. doi:10.1083/jcb.200407158

Zlokovic, B.V. 2008. The blood-brain barrier in health and chronic neurodegenerative disorders. *Neuron*. 57:178–201. doi:10.1016/j.neuron.2008.01.003